Patterned Arrays of Supramolecular Microcapsules **

Jing Zhang, [a,b‡] Ji Liu, [c‡] Ziyi Yu, [a] Su Chen, [b] Oren A. Scherman [c*] and Chris Abell [a*] **

Abstract *Micropatterning of hydrogel has brought innovative outcomes in fundamental and applied material sciences. Previous approaches have mainly been dedicated to fabricate arrays of bulk hydrogel beads, which have inherent challenges including loading ability, scalability, specificity and versatility. Here we present a methodology to create hollow microcapsule arrays from sessile microdroplets. The difference in wettability between hydrophilic and hydrophobic surfaces enables self-partitioning of liquid into microdroplet arrays, serving as microreservoirs to load complementarily-functionalized host-guest polymers, cucurbit[8]uril-threaded highly-branched polyrotaxanes (HBP-CB[8]) and naphthyl-functionalized hydroxyethyl cellulose (HEC-Np). The interfacial dynamic complexation between positively-charged HBP-CB[8] and HEC-Np occurred in the presence of negatively-charged surfactants, resulting in condensed supramolecular hydrogel skins. The hydrogel microcapsules were uniform in size, and were developed to encapsulate target cargos in a robust and well-defined manner. Moreover, the microcapsule substrates were further used for surface enhanced Raman spectroscopy (SERS) sensing upon loading of gold nanoparticles. This facile assembly of microcapsule arrays has potential applications in controlled cargo delivery, bio-sensing, high throughput analysis and sorting.*

Stimuli-responsive hydrogels are water-swollen three-dimensional polymer networks, and they have been extensively studied on account of their sensitivity to environmental stimuli including change in pH, light, mechanical stress, as well as thermal and electric triggers.[1–8] The capability to engineer bulk hydrogel materials into microarrays is promising for the development of miniaturized devices as controlled delivery systems, sensors, diagnostics and in tissue engineering.[9–16] Moreover, they enable extremely small-volume, high-throughput and compartmental manipulations. Such hydrogel compartmentalization can be readily designed from various stimuli-responsive polymers, imparting the microarrays with responsiveness/adaptability to environmental changes. Although this fabrication process has been extensively investigated, considerable efforts are dedicated to bulk hydrogel beads or patterns for capturing chemical or biological samples.[17–19] Patterned arrays made of hydrogel microcapsules have been rarely reported, due to the difficulty of accumulating polymer backbones at the microdroplet surface during the gelation process, unless a multiple emulsion technique is used.[20,21] Such hydrogel microcapsules are highly desirable, on account of their unique characteristics such as hollow cavities, well-defined skins as well as relatively large space available for cargo encapsulation and isolated reactions.[22–26]

In this study we exploit supramolecular building units to construct patterned hydrogel microcapsules on solid substrates for cargo delivery and chemical sensing. Supramolecular materials are built through non-covalent interactions such as metal coordination, hydrogen bonding, ionic interactions, π-π stacking or host-guest interactions.[22,27–29] In our previous report, supramolecular microcapsules can be readily fabricated through a *one-step* microfluidic approach.[30–32] Complementarily-functionalized polymers in an aqueous phase accumulated at the water/oil interface with the presence of charged surfactants.[22] Dynamic CB[8] host-guest complexation between these polymers then yielded well-defined microcapsule skins. This supramolecular interaction is potentially responsive to a wide variety of stimuli, such as redox, light, competitive guests and temperature.[22,29,33,34]

Self-partitioned sessile microdroplets are used here to locally accommodate supramolecular polymers and pattern the hydrogel microcapsules. In addition to properties associated with mobile microfluidic droplets, *e.g.* low reagent consumption and high throughput, sessile microdroplets exhibit exceptional advantages such as controllable morphology, allowance for facile tracking and manipulation.[23–26] Briefly, a glass slide was treated with piranha solution to remove any possible contaminants (**Figure 1a**), followed by the surface functionalisation with trichloro(1*H*, 1*H*, 2*H*, 2*H*-perfluorooctyl)silane, yielding a hydrophobic surface with a contact angle of 110°. A further hydrophilic micropattern was generated through oxygen plasma treatment with a polydimethylsiloxane (PDMS) mask. Due to the wettability difference between the non-treated (hydrophobic) and

** J.Z. thanks the Priority Academic Program Development of Jiangsu Higher Education Institutions (PAPD) and Natural Science Foundation of Jiangsu Province (BK20171013) for financial support. J.L. is financially supported by the Marie Curie FP7 SASSYPOL ITN (607602) program. O.A.S thanks the EPRSC (EP/F0355351 and EP/G060649/1) and ERC (ASPiRe, 240629) for their funding.

* [a] Department of Chemistry, University of Cambridge, Lensfield Road, Cambridge CB2 1EW, UK.
E-mail: zy251@cam.ac.uk, ca26@cam.ac.uk.
[b] State Key Laboratory of Materials-Oriented Chemical Engineering, College of Chemical Engineering, Nanjing Tech University, Nanjing, 210009, P. R. China.
[c] Melville Laboratory for Polymer Synthesis, Department of Chemistry, University of Cambridge, Cambridge, CB2 1EW, United Kingdom.
E-mail: oas23@cam.ac.uk. .
‡ These authors contribute equally in this work.

Supporting information for this article is available on the WWW under or from the author.

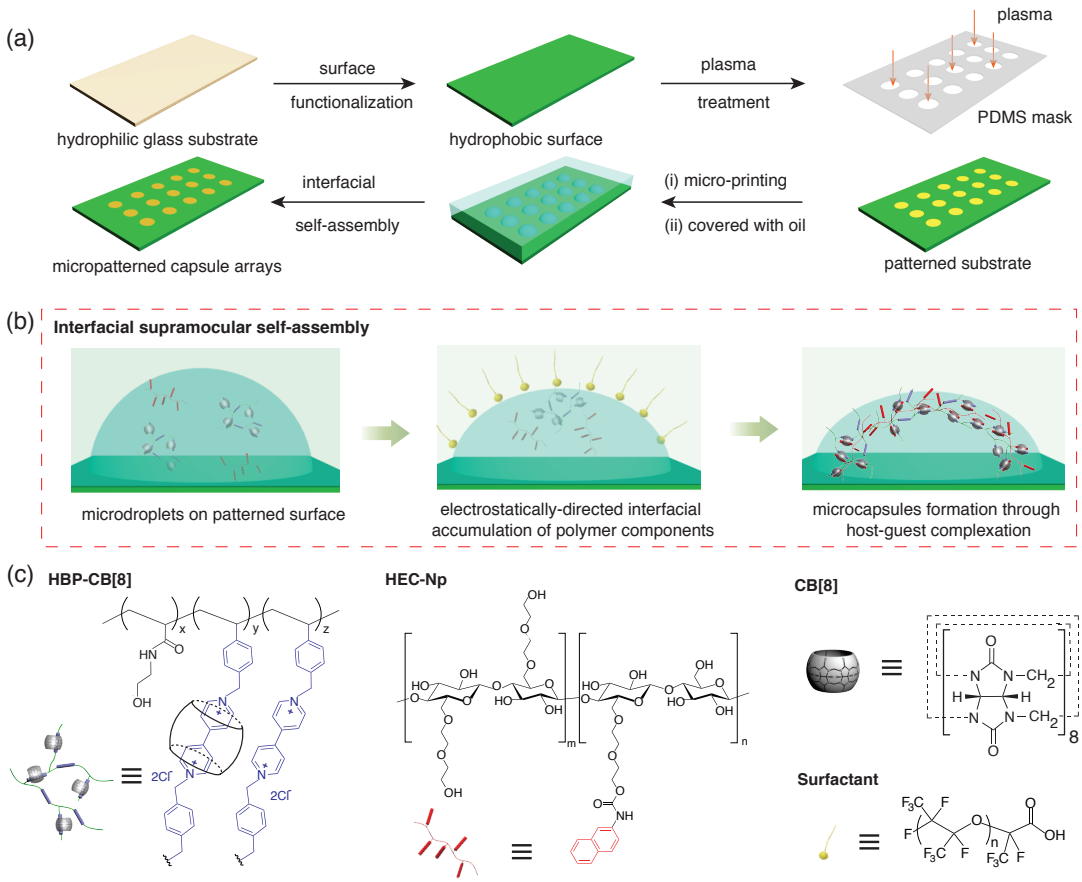

Figure 1. Schematic illustration for preparing the patterned arrays of supramolecular hydrogel-based microcapsules. (**a**) Construction of wettability-tunable glass substrates to prepare microdroplet arrays and subsequent in situ formation of supramolecular hydrogel microcapsule arrays; (**b**) interface self-assembly of supramolecular components to achieve hydrogel microcapsules and (**c**) chemical structures of the components used here.

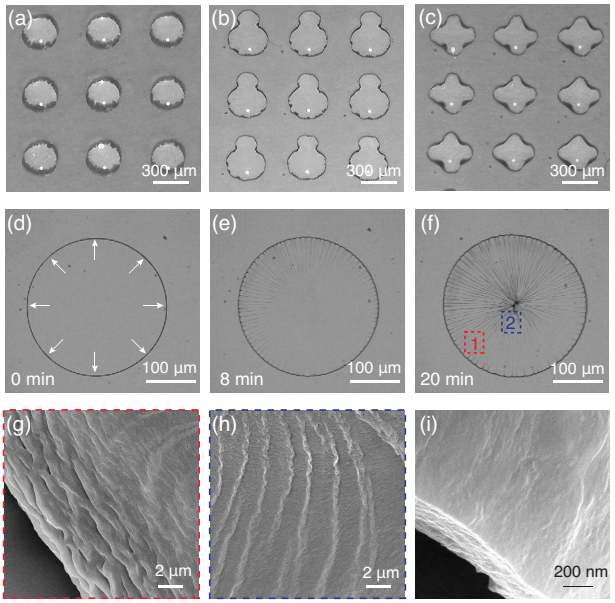

Figure 2. Supramolecular microcapsule array generated through the wettability-mediated assembly strategy. (**a**-**c**) Optical images of the as-obtained microdroplets arrays with spherical, snowman and cross morphologies, respectively. (**d**-**f**) Bright-field images of the dynamic assembly process for the hemispheric supramolecular hydrogel microcapsules. (**g**-**h**) SEM images of Area 1 and Area 2 in (**f**), and (**i**) its cross-sectional view of the resulting supramolecular hydrogel microcapsules.

treated (hydrophilic) areas, aqueous solutions could readily form an array of sessile microdroplets on the patterned hydrophilic areas. The microdroplet surfaces were then covered with a layer of oil, in order to guide the supramolecular self-assemblies at the oil/water interface and control the water evaporation.

Sessile microdroplets containing a mixture of highly-branched HBP-CB[8] and HEC-Np (chemical structures listed in **Figure 1c**) were used here to form the microcapsules. To tune the interfacial assembly, Fluorinert oil (3M, FC-40) containing 1.8 *wt.%* negatively-charged dopant of Krytox® 157FS-L was used. On account of the electrostatic interactions between the positively-charged HBP-CB[8] (microdroplets) and complementarily-charged perfluorinated dopant (oil phase), the polymer components preferentially accumulated at the droplet interface.[22,35] Additionally, CB[8]-mediated host-guest complexation between HBP-CB[8] and HEC-Np promoted the formation of a hydrogel skin as well as the supramolecular capsule arrays (**Figure 1b**). The strong yet dynamic CB[8] host-guest interactions impart the hydrogel skins with additional properties, such as stimuli-responsiveness, adaptiveness and self-healing, which will be explored in the following context.

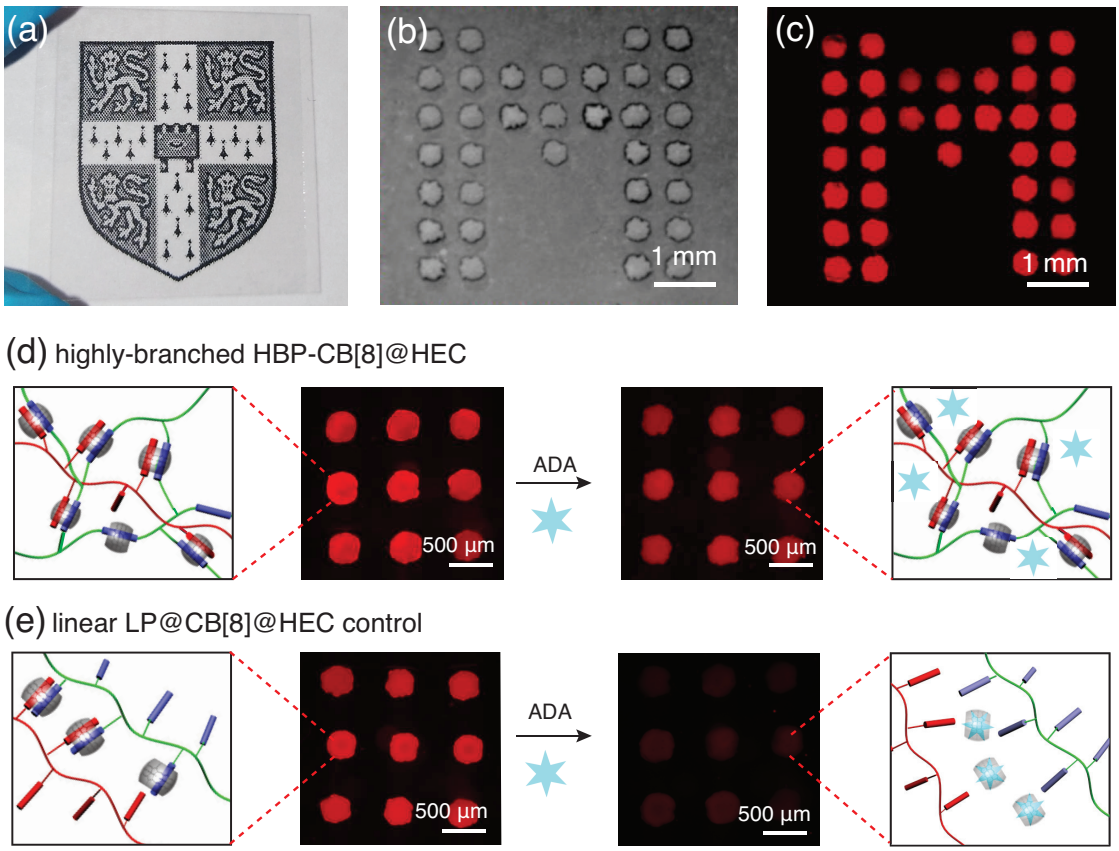

Figure 3. Cargo retention capacity of the supramolecular hydrogel microcapsule arrays. (**a**) An optical image of the rehydrated capsule arrays, showing high transparency with a Cambridge University logo as background. The optical (**b**) and fluorescence (**c**) images of the TRITC-dextran-loaded capsules upon adding a drop of water. Cargo retention capacity of (**d**) highly-branched HBP-CB[8]@HEC microcapsule arrays, with (**e**) the linear analogue LP@CB[8]@HEC as a control, upon immersing into the aqueous ADA solution (1 mM). Competitive guest (ADA) could effectively dissociated the ternary complexes within the LP@CB[8]@HEC as a control, but not the highly-branched HBP-CB[8]@HEC, on account of the mechanical locking of the CB[8] host molecules.

Microcapsule arrays with controllable sizes and patterns could be achieved using sessile microdroplets. As shown in **Figure 2a-c**, microdroplet arrays in the shape of spheres, snowmen and crosses could be readily generated by simply defining the hydrophilic patterns. This feature makes it possible to encode useful information within these individual compartments, removing reliance on fluorescent labelling. Due to the strong adhesion between the polymeric components and the glass substrate, coating with high-density perfluorinated oil (1.85 g cm^{-3}) does not cause the delamination and floating of the microdroplets, but rather stabilizes the micropatterns and facilitated the interfacial self-assembly while the water slowly evaporated (**Figure 2d-f**). *In situ* observation shows the evolution from transparent and homogeneously-distributed microdroplets (**Figure 2d**, polymer solution), through the appearance of wrinkle and buckles at the edges (**Figure 2e**, formation of supramolecular hydrogel shells upon water evaporation), and finally a polymer skin on the supramolecular hydrogel microcapsules arrays (**Figure 2f**, completion of water evaporation).

The complementarily-charged dopant and the perfluorinated oil together play a critical role on the formation of microcapsules. In addition to providing the interface for complexation, the oil layer also suppresses the capillary flow from the droplet centre to its edge, ensuring uniform distribution, other than the coffee-ring effect, of polymer components throughout the entire droplet during water evaporation.[36,37] Subsequently, supramolecular hydrogel skin formed at the micropatterned areas (thickness of *ca.* 300 nm), and appearance of folds and creases was noticed due to shrinkage during water evaporation (**Figure 2g-i**). On the other hand, microcapsules could also be readily accessed through the free standing microdroplets via the microfluidic technique (see **ESI Figure S1**), similar to our previous reports,[30–32] further confirming the electrostatic interaction as a driving force for hydrogel skin generation.

Simultaneous encapsulation of guest molecules during microdroplet formation provides a facile method for cargo loading, as well as subsequent controlled release. To generate cargo-loaded microcapsules, tetramethylrhodamine isothiocyanate-dextran (TRITC-dextran, 155 kDa) was directly added with a mixture solution of HEC-Np and HBP-CB[8] prior to the wettability-based microdroplet deposition process. Upon loading, the cargos were encapsulated within the aqueous microdroplets and located within the core of the microcapsules. **Figure 3a** shows the as-obtained cargo-loaded microcapsule arrays after rehydration. Due

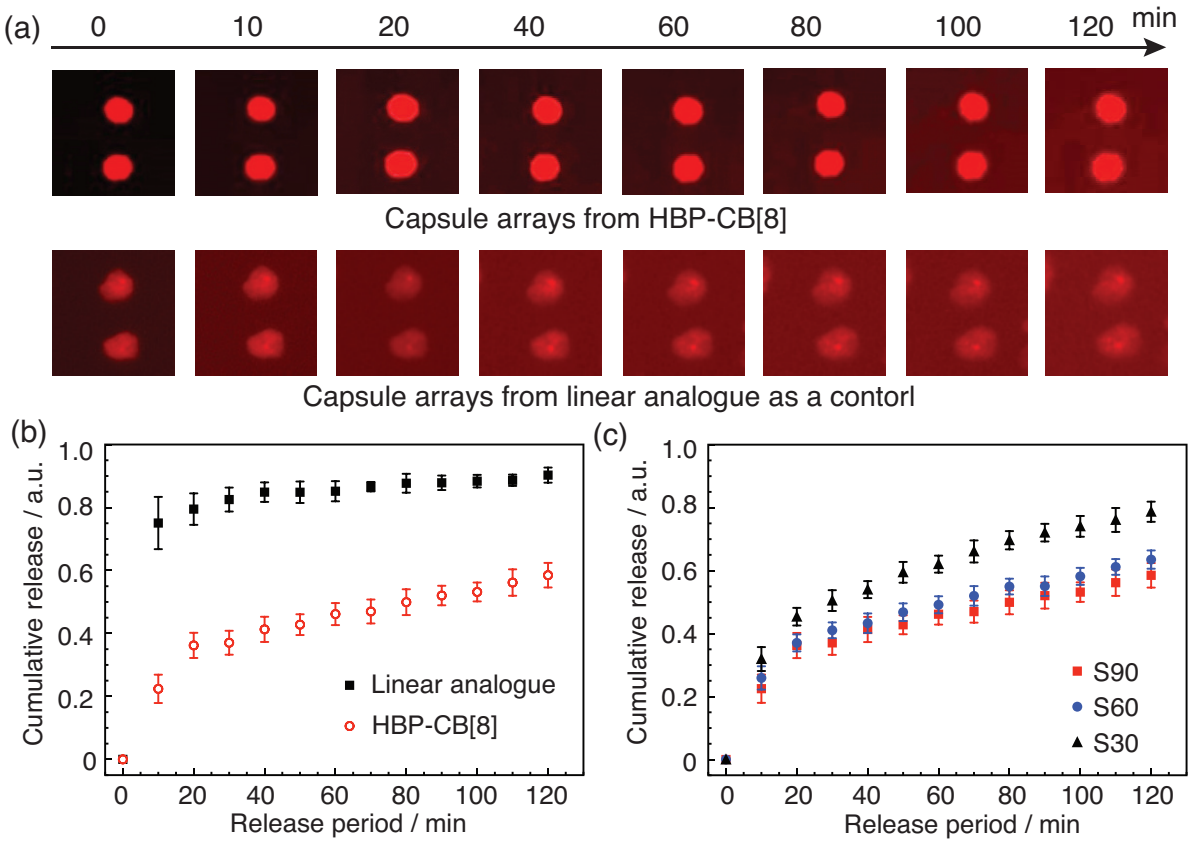

Figure 4. Cargo release performance of the supramolecular hydrogel microcapsule arrays. (**a**) Fluorescence micrographs of cargo-loaded microcapsule arrays after rehydration. (**b**) Release profiles of the cargo-loaded microcapsule arrays including CB[8]@LP arrays and highly-branched HBP-CB[8] microcapsules arrays, respectively. (**c**) The effect of concentration of supramolecular forming components on the cargo retention capacity of the as-obtained highly-branched HBP-CB[8] microcapsule arrays. Note: S30, S60 and S90 refer to HBP-CB[8]@HEC microcapsules assembled from 30, 60 and 90 μM CB[8] crosslinking motifs, respectively.

to the similar refractive indices between the glass substrate and polymer components, these microcapsule arrays became transparent. After exposure to a drop of water, the patterned areas transformed into hemispherical microdroplet arrays upon hydration (**Figure 3b**), with remarkable red fluorescence observed (**Figure 3c**), due to the retention of TRITC-dextran cargo upon rehydration. To evaluate the robustness of the microcapsules built with highly-branched HBP-CB[8] backbones, exposure to 1-aminoadamantane (ADA), a competitive guest for MV^{2+}·Np·CB[8] ternary complexes,[22,28,29] was conducted. Because of the mechanical locking of CB[8] host molecules onto the polymer backbone,[38] the ADA molecules could not effectively dissociate the complexes (**Figure 3d**). On the contrary, for a control made of its analogue linear poly(HEAm-*co*-StMV), addition of ADA readily destructing the microcapsule structure and inducing an burst release of TRITC-dextran (**Figure 3e**).

To further investigate the molecular permeability of the microcapsule arrays, release kinetics of the TRITC-dextran cargos were tracked over time. As shown in **Figure 4a**, cargo within HBP-CB[8]@HEC microcapsules was retained for a longer period than the linear controls. The TRITC-dextran cargo rapidly released from the linear polymer arrays, with almost 80% release within the first 10 min (**Figure 4b**). On the contrary, 20% release was detected in the first 10 min for the HBP-CB[8]@HEC microcapsules arrays, followed by a steady release profile with a 50% release over 2 h. This release character indicates that the highly-branched geometry improved the cargo retention capacity substantially. One of the attractive features of the HBP-CB[8] arises from its high CB[8] loading capacity, without sacrificing its aqueous solubility ($C_{CB[8]} > 20$ mM). Moreover, the branched chain topology remarkably increased the characteristic relaxation time (τ_c) of the hydrogel network by over 5 orders of magnitude through a spatiotemporal tuning, thus enhanced mechanical strength, as well as decreased porous size here.[38,39] A further investigation was carried out to study the effect of polymer loading amounts on the cargo retention capacity. S30, S60 and S90 (**Figure 4c**) correspond to release profiles of HBP-CB[8]@HEC microcapsules assembled from 30 μM, 60 μM and 90 μM CB[8] crosslinking motifs, respectively. A burst release of 20% was also observed at the early stage of rehydration, with subsequent sustainable release. Surprisingly, as the amount of polymeric components increases, a faster release was detected, which is something that warrants further investigation.

In addition, the microcapsule arrays were capable of immobilizing gold nanoparticles onto their surfaces, facilitating SERS sensing (**Figure 5a**).[40] Gold naoparticles (diam-

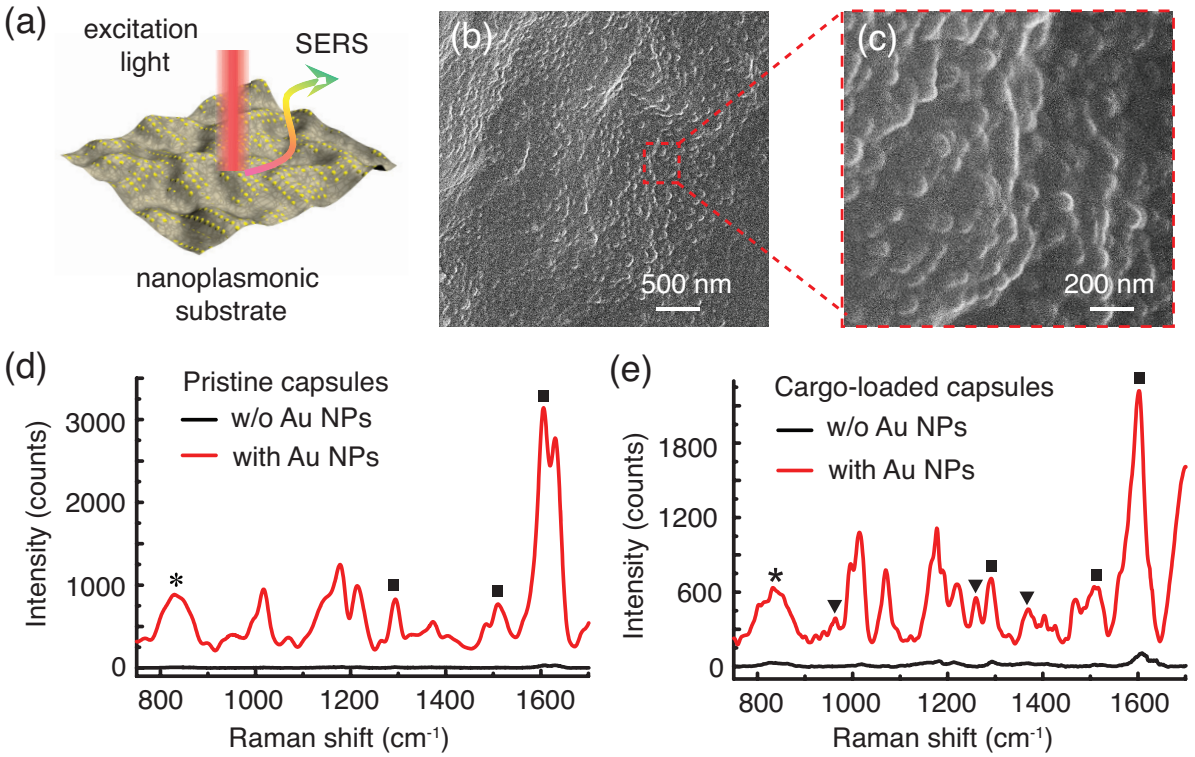

Figure 5. (**a**) Surface enhanced Raman spectroscopy (SERS) substrate derived from gold nanoparticles (Au NPs) attached to microcapsule arrays. (**b** and **c**) SEM images for patterned capsules after immersing into an aqueous solution containing Au NPs. (**d**) SERS spectra of capsule arrays with no Au NPs (black line), Au NPs covered capsule arrays (red line); (**e**) SERS spectra of TRITC-dextran encapsulated microcapsules without (black line) and with Au NPs (red line).

eter: 60 nm) were immobilized onto the microcapsule skins (**Figure 5b** and **5c**). The Raman spectra were recorded in a backscattering geometry (wavelength of 633 nm, power of 55 μW and acquisition time of 100 ms). The Raman spectra of the microcapsule sample without Au NPs (control, black line in **Figure 5d**) shows a very low-intensity Raman band. Nevertheless, with Au NPs immobilized, enhanced signals centred at *ca.* 830 cm^{-1} (characteristic peak for CB[8]), 1630, 1560 and 1308 cm^{-1} (characteristic peaks for MV^{2+}) were readily detected (red line in **Figure 5d**).[41] Significantly, the cargo-loaded capsules (TRITC-dextran, 5 μM) could also be probed by SERS. **Figure 5e** shows the SERS spectra of TRITC-dextran encapsulated microcapsules before and after Au NP immobilization. It reveals that the characteristic peaks of TRITC-dextran cargo centered at 962, 1260 and 1367 cm^{-1} could be readily distinguished after the immobilization of Au NPs. It is also worth pointing out that immobilization of Au NPs did not interfere with capsule formation or the cargo-loading process, which would be important for sensing in application involving cell culture and/or precise microreactions.

We have developed a sessile microdroplet deposition method that allows for preparing patterned arrays of supramolecular hydrogel microcapsules on a solid substrate. This methodology is based on the difference in wettability between the hydrophilic and hydrophobic patterned areas, where self-separated microdroplets can be generated in a facile and high throughput manner. By combining dynamic cucurbit[*n*]uril host-guest chemistry and electrostatically-directed interfacial self-assembly, the formation of a supramolecular hydrogel skin at the microdroplet interface has been demonstrated. The simultaneous delivery of capsule-forming building blocks and cargo enables encapsulation of cargo during microdroplet formation. Furthermore, the microcapsule arrays provide a methodology to perform parallel detection, as demonstrated by SERS measurements. Given the wide range of dynamic chemistries that can be exploited for supramolecular assemblies, we envision that this sessile microdroplet platform will inspire a number of supramolecular fabrication techniques. Moreover, the miniaturization of conventional analytical systems for novel diagnostics or therapeutics, which require a high-throughput cargo loading and encoding capacity, may benefit from this approach.

Experimental section

General: images of microdroplet formation were captured using a Phantom v7.2 camera, attached to an Olympus IX71 inverted microscope. Laser scanning confocal microscope (LSCM) measurements were carried out using a Leica TCS SP5 confocal microscope. Microscopic images and fluorescence images were obtained using an Olympus IX81 inverted optical microscope coupled with a camera of Andor Technology EMCCD iXonEM+ DU 897. Scanning electron

microscopy (SEM) measurements were made and images recorded using a Leo 1530 variable pressure SEM with InLens detector. ^{1}H NMR spectra (500 MHz) were collected on a Bruker Avance QNP 500 MHz ultrashield spectrometer, equipped with a 5-mm BBO ATM probe with a *z*-gradient. All starting chemicals were purchased from Sigma Aldrich and used as received unless stated otherwise. Microfluidic devices were designed according to our previously reported method.[30,31] All aqueous solutions were prepared with deionized water treated with a Milli-Q TM (18 mΩ cm^{-1}).

Synthesis of HEC-Np: the HEC-Np was prepared following the previously-reported protocol.[33] Specifically, hydroxyethylcellulose (HEC, 1.00 g) was dissolved in N-methylpyrrolidone (NMP, 120 mL) at 110 °C overnight. The solution was cooled to room temperature and 2-naphthyl isocyanate (Np-NCO, 29.7 mg, 0.18 mmol) and dibutyltin dilaurate (TDL, 3 drops) were added, and the mixture was left stirring for overnight at room temperature. The crude product was then purified by precipitation into acetone for three times, filtered, and dried overnight under vacuum at 60 C (1.01 g, 98%). For the synthesis of rhodamine B-labeled HEC-Np, rhodamine B isocyanate (1 mg, 2 μmol) was added, during the reaction between the reaction of HEC and 2-naphthyl isocyanate, following the same protocol.

Synthesis of highly branched CB[8]-threaded polyrotaxanes, HBP-CB[8]: a semi-batch RAFT polymerisation was conducted to synthesize the HBP-CB[8] copolymers.[38,39] Specifically, *N*-hydroxylethyl acrylamide (HEAm) and chain transfer agent benzyltrithiocarbonyl propionic acid (BCPA) were added into a flask with a feeding molar ratio of 50:1 (HEAm:BCPA). After N_2 was bubbled through the solution for at least 30 min, the polymerisation system was heated to 70 °C. A mixture of St-MV^{2+}-St and CB[8] (1:1 *mol.*) mixture was continuously fed into the reaction system at a constant rate during the polymerization. Upon the completion of adding St-MV^{2+}-St/CB[8] mixture, the polymerisation was continued at 70 °C for another 2 h, prior to quenching with liquid nitrogen. The crude polymer solution was precipitated in acetone, and further dialysis in a Spectra/Pro® membrane (MWCO: 6000 g mol^{-1}) against 1-adamantane amine solution (2 days) and subsequently, milli-Q water (3 days). Purified polymer was further freeze-dried, yielding a yellow amorphous solid (yield, *ca.* 90%). For FITC-labeled HBP-CB[8], HBP-CB[8] polymer (0.4 g) and fluorescein isocyanate (0.1 *mol.%* of hydroxyl group in HBP-CB[8]) was dissolved in DMSO, and reacted for overnight with TDL as catalysis. The crude product was purified through 3-day dialysis (MWCO: 6,000 g mol^{-1}), followed with freeze-drying (yield, *ca*. 95%).

Synthesis of linear poly(HEAm-co-StMV), LP: HEAm (2.00 g, 17.00 mmol), St-MV^{2+} (0.382 g, 0.85 mmol), 2,2'-azobis-(2-methylpropionitrile) (16.8 mg, 0.1 mmol) and BCPA as CTA were dissolved in a mixture of DMSO:EtOH (10:4 *vol.* to make a total volume of 14 mL). The solution was bubbled with N_2 for 30 min and then heated to 70 °C for 48 h. The polymer was then precipitated in diethyl ether and then THF before vacuum drying to yield yellow solid (yield, 89%).

Preparation of supramolecular microcapsules through microfluidic chips: two different liquids, loaded on two separated syringe pumps (PHD, Harvard Apparatus), were injected into a microfluidic device to generate water-*in*-oil microdroplets. Flourinert oil (3M, FC-40) containing a 2.0 *wt.%* fluorous surfactant (XL-171, Sphere Fluidics *Ltd.*) and 1.8 wt.% Krytox® 157FS-L was used as the continuous phase. Discontinuous phase was prepared by dissolving certain amount of HBP-CB[8] and HEC-Np in water. The continuous phase and discontinuous phase solutions were loaded into two separate 1 mL syringes, before connecting to the microfluidic chip. Syringes with needles were mounted on syringe pumps and fitted with polyethylene tubing, while the other end of the tube was inserted into the appropriate inlets of a microfluidic chip. In order to generate microdroplets, Flourinert FC-40 was first pumped into the device at a rate of 200 μL h^{-1} to fill the appropriate channels. The aqueous dispersed phase was then pumped into the device at 100 μL h^{-1}. Monodispersed microdroplets were generated as the oil phase sheared off the aqueous phase. In a typical experiment, the concentration of HBP-CB[8] and HEC-Np were set at 30 μM of CB[8], with an equal molar ratio of CB[8]:Np. The as-obtained microdroplets were transferred to petri dish, followed by a further 5-h dehydration, yielding isolated microcapsules.

Molecule permeability evaluation: to evaluate the molecular permeability, the cargo-loaded microcapsules were washed with HFE-7500 three times to remove the residual surfactants after drying on a glass bottom dish. The glass bottom dish was sealed with parafilm and mounted on the fluorescence microscope after a few drops of water were smeared over the dried microcapsules. The fluorescent images were taken every 10 min over 2 h. For the quantitative analysis of the cargo release, fluorescent intensities recorded from three different locations within a fluorescence image were used to give an averaged value.

References

[1] L. D. Zarzar, P. Kim, J. Aizenberg, *Adv. Mater.* **2011**, *23*, 1442–1446.

[2] R. F. Donnelly, T. R. R. Singh, M. J. Garland, K. Migalska, R. Majithiya, C. M. McCrudden, P. L. Kole, T. M. T. Mahmood, H. O. McCarthy, A. D. Woolfson, *Adv. Funct. Mater.* **2012**, *22*, 4879–4890.

[3] F. Fu, Z. Chen, Z. Zhao, H. Wang, L. Shang, Z. Gu, Y. Zhao, *Proc. Natl. Acad. Sci. USA* **2017**, *114*, 5900–5905.

[4] Y. S. Kim, M. Liu, Y. Ishida, Y. Ebina, M. Osada, T. Sasaki, T. Hikima, M. Takata, T. Aida, *Nat. Mater.* **2015**, *14*, 1002–1007.

[5] J. Liu, C. S. Y. Tan, Z. Yu, Y. Lan, C. Abell, O. A. Scherman, *Adv. Mater.* **2017**, *29*, 1604951.

[6] H. Shao, C.-F. Wang, J. Zhang, S. Chen, *Macromolecules* **2014**, *47*, 1875–1881.

[7] J. Zhang, S. Yang, Y. Tian, C.-F. Wang, S. Chen, *Chem. Commun.* **2015**, *51*, 10528–10531.

[8] Z. Yu, C.-F. Wang, L. Ling, L. Chen, S. Chen, *Angew. Chem. Int. Ed.* **2012**, *51*, 2375–2378.

[9] Y. Li, P. Chen, Y. Wang, S. Yan, X. Feng, W. Du, S. A. Koehler, U. Demirci, B.-F. Liu, *Adv. Mater.* **2016**, *28*, 3543–3548.

[10] J. Liu, H. Guo, B. Zhang, S. Qiao, M. Shao, X. Zhang, X.-Q. Feng, Q. Li, Y. Song, L. Jiang, J. Wang, *Angew. Chem. Int. Ed.* **2016**, *128*, 4337–4341.

[11] F. Xu, J. Wu, S. Wang, N. G. Durmus, U. A. Gurkan, U. Demirci, *Biofabrication* **2011**, *3*, 034101.

[12] N. Suzuki, E. Iwase, H. Onoe, *Langmuir* **2017**.

[13] H. Kim, R. E. Cohen, P. T. Hammond, D. J. Irvine, *Adv. Funct. Mater.* **2006**, *16*, 1313–1323.

[14] J. Hou, M. Li, Y. Song, *Angew. Chem. Int. Ed.* **2018**, *in press*, DOI: 10.1002/anie.201704752.

[15] J. Hou, H. Zhang, Q. Yang, M. Li, Y. Song, L. Jiang, *Angew. Chem. Int. Ed.* **2014**, *53*, 5791–5795.

[16] J. Sun, B. Bao, M. He, H. Zhou, Y. Song, *ACS Appl. Mater. Interfaces* **2015**, *7*, 28086–28099.

[17] C.-H. Choi, H. Lee, A. Abbaspourrad, J. H. Kim, J. Fan, M. Caggioni, C. Wesner, T. Zhu, D. A. Weitz, *Adv. Mater.* **2016**, *28*, 3340–3344.

[18] A. M. Costa, J. F. Mano, *J. Am. Chem. Soc.* **2017**, *139*, 1057–1060.

[19] Y. J. Kang, H. S. Wostein, S. Majd, *Adv. Mater.* **2013**, *25*, 6834–6838.

[20] A. Utada, E. Lorenceau, D. Link, P. Kaplan, H. Stone, D. Weitz, *Science* **2005**, *308*, 537–541.

[21] H. Ke, J. Wang, Z. Dai, Y. Jin, E. Qu, Z. Xing, C. Guo, X. Yue, J. Liu, *Angew. Chem. Int. Ed.* **2011**, *123*, 3073–3077.

[22] J. Liu, Y. Lan, Z. Y. Yu, C. S. Y. Tan, R. M. Parker, C. Abell, O. A. Scherman, *Acc. Chem. Res.* **2017**, *50*, 208–217.

[23] A. A. Popova, S. M. Schillo, K. Demir, E. Ueda, A Nesterov-Mueller, P. A. Levkin, *Adv. Mater.* **2015**, *27*, 5217–5222.

[24] A. I. Neto, K. Demir, A. A. Popova, M. B. Oliveira, J. F. Mano, P. A. Levkin, *Adv. Mater.* **2016**, *28*, 7613–7619.

[25] R. J. Jackman, D. C. Duffy, E. Ostuni, N. D. Willmore, G. M. Whitesides, *Anal. Chem.* **1998**, *70*, 2280–2287.

[26] F. L. Geyer, E. Ueda, U. Liebel, N. Grau, P. A. Levkin, *Angew. Chem. Int. Ed.* **2011**, *50*, 8424–8427.

[27] M. Nakahata, Y. Takashima, H. Yamaguchi, A. Harada, *Nat. Commun.* **2011**, *2*, 511.

[28] L. Yang, X. Tan, Z. Wang, X. Zhang, *Chem. Rev.* **2015**, *115*, 7196–7239.

[29] J. Liu, C. S. Y Tan, Y. Lan, O. A. Scherman, *Macromol. Chem. Phys.* **2016**, *217*, 319–332.

[30] J. Zhang, R. J. Coulston, S. T. Jones, J. Geng, O. A. Scherman, C. Abell, *Science* **2012**, *335*, 690–694.

[31] Y. Zheng, Z. Yu, R. M. Parker, Y. Wu, C. Abell, O. A. Scherman, *Nat. Commun.* **2014**, *5*, 5772.

[32] Z. Yu, J. Zhang, R. J. Coulston, R. M. Parker, F. Biedermann, X. Liu, O. A. Scherman, C. Abell, *Chem. Sci.* **2015**, *6*, 4929–4933.

[33] C. S. Y. Tan, J. del Barrio, J. Liu, O. A. Scherman, *Polym. Chem.* **2015**, *6*, 7652–7657.

[34] J. Liu, C. S. Y. Tan, Z. Y. Yu, N. Li, C. Abell, O. A. Scherman, *Adv. Mater.* **2017**, *29*, 1605325.

[35] R. M. Parker, J. Zhang, Y. Zheng, R. J. Coulston, C. A. Smith, A. R. Salmon, Z. Yu, O. A. Scherman, C. Abell, *Adv. Funct. Mater.* **2015**, *25*, 4091–4100.

[36] P. J. Yunker, T. Still, M. A. Lohr, A. Yodh, *Nature* **2011**, *476*, 308–311.

[37] H. Fudouzi, *Colloids Surf. Physicochem. Eng. Asp.* **2007**, *311*, 11–15.

[38] C. S. Y. Tan, J. Liu, A. S. Groombridge, S. J. Barrow, C. A. Dreiss, O. A. Scherman, *Adv. Funct. Mater.* **2018**, *28*, 1702994.

[39] Z. Yu, J. Liu, C. S. Y. Tan, O. A. Scherman, C. Abell, *Angew. Chem. Int. Ed.* **2018**, *in press*, DOI: 10.1002/anie.201711522.

[40] S. Kasera, F. Biedermann, J. J. Baumberg, O. A. Scherman, S. Mahajan, *Nano Lett.* **2012**, *12*, 5924–5928.

[41] R. W. Taylor, T.-C. Lee, O. A. Scherman, R. Esteban, J. Aizpurua, F. M. Huang, J. J. Baumberg, S. Mahajan, *ACS Nano* **2011**, *5*, 3878–3887.

Entry for the Table of Contents (Please choose one layout only)

Layout 1:

Patterned Arrays of Supramolecular Microcapsules

Jing Zhang, [a,b‡] *Ji Liu,* [c‡] *Ziyi Yu,* [a*] *Su Chen,* [b] *Oren A. Scherman* [c*] *and Chris Abell* [a*]

Patterned Arrays of Supramolecular Microcapsules

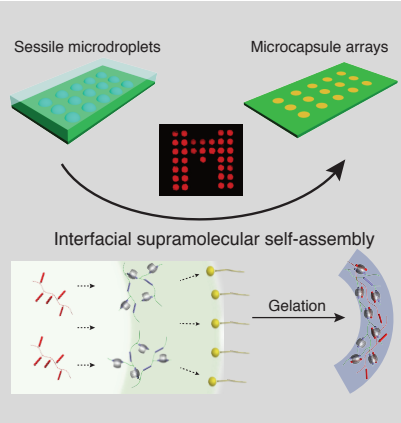

Formation of patterns of supramolecular microcapsules from highly branched CB[8]-threaded polyrotaxane (HBP-CB[8]) and naphthyl-functionalized hydroxyethyl cellulose HEC (HEC-Np), through the wettability-mediated printing process. The interfacial dynamic complexation between positively-charged HBP-CB[8] and HEC-Np occurred under the assistance of negatively-charged surfactants, resulting in condensed yet dynamic supramolecular microcapsule skin.

Layout 2:

Catch Phrase:

Author(s), Corresponding Author(s) . . . . . Page Page*

Title Text

((The TOC Graphic should not exceed the size of this area))

Text for Table of Contents, max. 450 characters.